Journal of Orthopaedic Translation 40 (2023) 116–131

Contents lists available at ScienceDirect

Journal of Orthopaedic Translation

journal homepage: www.journals.elsevier.com/journal-of-orthopaedic-translation

Original Article

Gli1 depletion induces oxidative stress and apoptosis of nucleus pulposus cells via Fos in intervertebral disc degeneration

Libangxi Liu [1], Yuyao Zhang [1], Jiawei Fu, Xuezheng Ai, Dan Long, Xue Leng, Yang Zhang, Bo Huang, Changqing Li [***], Yue Zhou [**], Chencheng Feng [*]

Department of Orthopedics, Xinqiao Hospital, Army Medical University, Chongqing, 400037, PR China

ARTICLE INFO

Keywords:
Oxidative stress
Apoptosis
Intervertebral disc degeneration
Gli1
Fos

ABSTRACT

Background: Intervertebral disc degeneration (IDD) is the most common chronic disease. Oxidative stress and apoptosis of nucleus pulposus (NP) cells disrupt intervertebral disc (IVD) homeostasis, which is the main cause of IDD. Glioma-associated oncogene 1 (Gli1) is an important transcription factor in the Hedgehog (Hh) pathway. Depletion of Gli1 accelerates the occurrence and development of degenerative diseases. This study aimed to explore the role of aging related Gli1 depletion in the progression of IDD.

Methods: The relationship between aging related Gli1 depletion and IDD was studied in the NP tissues of human and rats of different ages, and the levels of oxidative stress and NP cell apoptosis during IDD were explored. Gli1 depletion of NP cells were established by targeting inhibitor GANT61 or lentivirus-coated Gli1 sh-RNA (sh-Gli1) to explore the role of Gli1 in NP cells and underlying mechanism. Exogenous Gli1 depletion induced IDD of rats was established by intraperitoneal injection of GANT61. Also, the roles of Fos in the Gli1 depletion induced NP cell oxidative stress, apoptosis and IDD were investigated.

Results: Gli1 was down-regulated in the tissues of degenerative NP, and the level of Gli1 was negatively correlated with the severity of aging related IDD in human and rats. Furthermore, we found enhanced oxidative stress and apoptosis in degenerative NP tissues. Gli1 depletion promoted oxidative stress and apoptosis of NP cells and resulted in the degradation of extracellular matrix (ECM) and decreased ECM synthesis. Transcriptome sequencing showed that Gli1 depletion caused Fos activation in NP cells. the effect of Gli1 depletion on the oxidative stress and apoptosis of NP cells were retarded by Fos inhibitor. In vivo, Fos inhibition alleviated the IDD induced by exogenous Gli1 depletion.

Conclusions: This study revealed for the first time that Gli1 is gradually depleted in NP with IDD progression. Exogenous Gli1 depletion causes oxidative stress and apoptosis of NP cells both in vivo and in vitro. Fos suppression effectively retards the destructive effects of Gli1 depletion on IVD homoeostasis.

The translational potential of this article: This study may provide new potential targets for preventing and reversing IDD. Maintaining Gli1 expression in NP and suppressing Fos activation may be an effective treatment strategy for IDD.

1. Introduction

Low back pain (LBP) is a leading cause of disability and labor loss and affects approximately 700 million people worldwide, which causes a serious reduction in quality of life and leads to significant medical costs [1]. More importantly, approximately 30% of patients of LBP converts to

Abbreviations: IDD, intervertebral disc degermation; NP, nucleus pulpous; IVD, intervertebral disc; Gli1, glioma-associated oncogene 1; ECM, extracellular matrix; LBP, low back pain; ACAN, aggrecan; Shh, sonic hedgehog; 4HNE, 4-hydroxynonenal; SD, sprague-dawley; 2M, 2-month-old; 10M, 10-month-old; 20M, 20-month-old; H&E, hematoxylin and eosin; ROS, reactive oxygen species; MDA, malondialdehyde; GPX, glutathione peroxidase; SOD, superoxide dismutase; MRI, magnetic resonance imaging; DEGs, differentially expressed genes; GO, gene ontogeny; KEGG, kyoto encyclopedia of genes and genomes; GSEA, gene set enrichment analysis.

* Corresponding author.
** Corresponding author.
*** Corresponding author.
E-mail addresses: changqli1970@126.com (C. Li), happyzhou@vip.163.com (Y. Zhou), doctorfgy@163.com (C. Feng).

[1] Libangxi Liu and Yuyao Zhang contributed equally to this work.

https://doi.org/10.1016/j.jot.2023.05.008
Received 8 December 2022; Received in revised form 1 April 2023; Accepted 19 May 2023
Available online 13 June 2023

chronic LBP (CLBP), and they cannot participate in normal work due to CLBP, resulting in a very large loss of social productivity [2,3]. The etiology of CLBP is complex and includes biological, psychological and social factors. Among these factors, intervertebral disc degeneration (IDD) is the main cause of CLBP [4,5]. Understanding the pathological process of IDD contributes to the identification of targets for the prevention and treatment of IDD [6,7].

Nucleus pulposus (NP) is a core component of intervertebral disc (IVD), which is rich in extracellular matrix (ECM) components such as collagen II and aggrecan (ACAN) [8]. NP plays an important role in the maintenance of IVD homeostasis due to its gelatinous structure and properties of elasticity and axial stress resistance [9]. The decrease in the number of functional NP cells leads to the disturbance of IVD homeostasis, and consequently promotes IDD [10]. Oxidative stress is mainly caused by an imbalance of the intracellular redox system. It affects the function and survive of NP cells by inducing DNA damage and activating oxidative stress-related signaling pathways [11,12]. On the one hand, oxidative stress inhibits ECM synthesis of NP cells and promotes the secretion of ECM degrading enzymes and a variety of inflammatory factors. On the other hand, oxidative stress leads to the apoptosis of NP cells [13,14]. As a result, the structural and functional homeostasis of IVDs is disturbed, which causes IDD. Therefore, elucidating the mechanism of oxidative stress and apoptosis of NP cells will provide a new perspective for the repair of degenerative IVDs.

The Sonic Hedgehog (Shh) pathway is involved in IVD development, growth, maturation and degeneration [15,16]. Glioma-associated oncogene 1 (Gli1) is the crucial transcription factor of Shh pathway and mediates the regulatory effects of the Shh pathway on embryonic development, tumorigenesis and degenerative diseases [17,18]. Recent studies have shown that Gli1 plays a key role in the occurrence and development of oxidative stress related diseases, such as endometrial hyperplasia, renal ischemia reperfusion injury and neurodegenerative diseases [19–21]. Gli1 is also involved in cell proliferation, apoptosis and differentiation [22]. During aging related IDD, Shh pathway is gradually suppressed, and Gli1 is significantly depleted. Dahia et al. suggested that Gli1 depletion was closely related to IDD occurrence [15]. However, the effect of Gli1 depletion on IDD and the underlying mechanism still need to be further investigated.

Herein, we aimed to investigating the effects of Gli1 depletion on the oxidative stress and apoptosis in NP cells as well as IVD homeostasis. Moreover, the molecular mechanism underlying these effects was also elucidated. This study provided a new insight into the critical role of Gli1 in the maintenance of IVD homeostasis.

2. Materials and methods

2.1. Reagents and antibodies

The following reagents were used: GANT-61 (HY-13901, MCE, USA), T5224 (HY-12270, MCE, USA).

The following antibodies were used: rabbit anti-caspase-3 Antibody (9662 S, Cell Signaling Technology, USA), rabbit anti-aggrecan (13880-1-AP, Proteintech, USA), rabbit anti-MMP13 (18165-1-AP, Proteintech, USA), rabbit anti-GPX4 (ab125066, Abcam, USA), rabbit anti-4-Hydroxynonenal (4HNE) (ab46545, Abcam, USA), rabbit anti-Lamin B1 (12987-1-AP, Proteintech, USA), rabbit anti-Collagen II (ab188570, Abcam, USA), mouse anti-Gli1 (sc-515,781, Santa Cruz, USA), mouse anti-Bax (sc-7480, Santa Cruz, USA), mouse anti-Fos (ab208942, Abcam, USA), mouse anti-SOD2 (sc-137,254, Santa Cruz, USA), mouse anti-KRT19 (sc-376,126, Santa Cruz, USA), mouse anti-CD24 (551,133, BD Pharmingen, USA), mouse anti-CD45 (550,566, BD Pharmingen, USA), mouse anti-CD90 (554,894, BD Pharmingen, USA), mouse anti-CD105 (sc-18838, Santa Cruz, USA) and mouse anti-GAPDH (60004-1-Ig, Proteintech, USA). The use and dilution concentration of antibodies in different experiments were shown in Table 1.

Table 1
Primary antibodies for experiment.

Primary Antibody	Catalog Number	Dilution Ratio	Source
mouse anti-GAPDH	60004-1-Ig	WB (1:50,000)	Proteintech Group, USA
rabbit anti-Lamin B1	12987-1-AP	WB (1:1000)	Proteintech Group, USA
rabbit anti-aggrecan	13880-1-AP	WB (1:1000) IF (1:200)	Proteintech Group, USA
rabbit anti-Collagen II	ab188570	WB (1:1000)	Abcam, USA
rabbit anti-MMP13	18165-1-AP	WB (1:1000)	Proteintech Group, USA
mouse anti-Gli1	sc-515,781	WB (1:500) IF (1:100)	Santa Cruz, USA
rabbit anti-GPX4	ab125066	WB (1:1000)	Abcam, USA
mouse anti-SOD2	sc-137,254	WB (1:500)	Santa Cruz, USA
rabbit anti-4HNE	ab46545	WB (1:1000)	Abcam, USA
rabbit anti-caspase 3	9662 S	WB (1:1000)	Cell Signaling Technology, USA
mouse anti-Bax	sc-7480	WB (1:1000)	Santa Cruz, USA
mouse anti-Fos	ab208942	WB (1:1000)	Abcam, USA
mouse anti-KRT19	sc-376,126	IF (1:100)	Santa Cruz, USA
mouse anti-CD24	551,133	FCM (1:100)	BD Pharmingen, USA
mouse anti-CD45	550,566	FCM (1:100)	BD Pharmingen, USA
mouse anti-CD90	554,894	FCM (1:100)	BD Pharmingen, USA
mouse anti-CD105	sc-18838	FCM (1:100)	Santa Cruz, USA

2.2. Human NP specimens

All human experimental protocols, including case retrospective analysis and NP specimen collection, were approved by the Ethics Committee of Second Affiliated Hospital, Army Medical University (2022-YD212-01). Human NP specimens were obtained from 30 specimen donors who underwent percutaneous endoscopic lumbar discectomy or microdiscectomy due to lumbar disc herniation or lumbar spinal stenosis and the characteristics of patients were showed in Table 2 (inclusion criteria: NP tissue removed by primary surgery for degenerative lumbar disc disease; exclusion criteria: NP tissue from patients with trauma, active infection, spinal tumors and spinal deformity). Signed informed consent forms were obtained from the patients. The NP specimens were processed according to their intended use.

2.3. In vivo studies

Male Sprague–Dawley (SD) rats (2-month-old (2M), 200 ± 20 g; 10-month-old (10M), 450 ± 45 g; 20-month-old (20M), 750 ± 75 g) were obtained from Animal Center of Xinqiao Hospital (Chongqing, China). The rats were fed under specific pathogen-free conditions. The in vivo experiments were conducted following the guidelines of the International Guiding Principles for Animal Research and approved by the Ethics Committee of Animal Care and Ethics Committee of Army Medical University (Army Medical University, AMUWEC2020088).

12 male SD rats (2-month-old) were randomly divided into the DMSO group (n = 6) and the GANT61 group (n = 6). In DMSO group, 0.5 ml dimethyl Sulfoxide (DMSO (1%, diluted in saline; D8371, Solarbio, China)) were injected once every three days for 60 days. Rats in GANT61 group were intraperitoneally injected with 0.5 ml GANT61 (20 mg/kg, dissolved in 1% DMSO diluted in saline) once every three days for 60 days. Then, the DMSO group was randomly divided into the DMSO + DMSO group (n = 3) and DMSO + T5224 group (n = 3). And the GANT61 group was randomly divided into the GANT61 + DMSO group (n = 3) and GANT61 + T5224 group (n = 3). In DMSO + T5224 group and GANT61 + T5224 group, 0.5 ml T5224 (60 mg/kg, dissolved in 1% DMSO diluted in saline) dissolved once every three days for 60 days. In DMSO + DMSO group and GANT61 + DMSO group, 0.5 ml DMSO (1%)

Table 2
Patient demographics.

Num.	Gender	Age	Surgical segment	Pfirrmann grading	Diagnosis	VAS score (preoperative)
1	male	15	L4/5	2	intervertebral disc herniation	0
2	male	19	L4/5	3	intervertebral disc herniation	2
3	male	20	L4/5	2	intervertebral disc herniation	4
4	male	20	L5/S1	2	intervertebral disc herniation	0
5	male	22	L4/5	2	intervertebral disc herniation, spinal stenosis	0
6	female	25	L5/S1	3	intervertebral disc herniation	3
7	male	25	L5/S1	2	intervertebral disc herniation	4
8	male	28	L5/S1	2	intervertebral disc herniation	0
9	male	31	L4/5	2	intervertebral disc herniation	2
10	male	33	L4/5	3	intervertebral disc herniation	4
11	male	36	L5/S1	3	intervertebral disc herniation	0
12	female	37	L4/5	4	intervertebral disc herniation	0
13	male	38	L4/5	3	intervertebral disc herniation	3
14	male	42	L4/5	4	intervertebral disc herniation	2
15	male	53	L5/S1	3	spinal stenosis	2
16	female	57	L4/5	4	spondylolisthesis, spinal stenosis	3
17	male	59	L5/S1	4	intervertebral disc herniation, spinal stenosis	8
18	male	61	L5/S1	4	spinal stenosis	0
19	male	65	L5/S1	4	intervertebral disc herniation, spinal stenosis	0
20	female	65	L5/S1	5	intervertebral disc herniation, spinal stenosis	3
21	female	66	L4/5	4	spinal stenosis	7
22	female	66	L5/S1	5	spinal stenosis	6
23	female	67	L5/S1	5	spondylolisthesis, spinal stenosis	6
24	male	68	L5/S1	4	intervertebral disc herniation, spinal stenosis	6
25	female	69	L5/S1	5	intervertebral disc herniation, spinal stenosis	7
26	male	76	L4/5	5	spondylolisthesis, spinal stenosis	8
27	male	78	L4/5	5	spinal stenosis	3
28	female	79	L4/5	5	intervertebral disc herniation, spinal stenosis	2
29	female	81	L5/S1	5	intervertebral disc herniation, spinal stenosis, spondylolisthesis	5
30	female	83	L4/5	5	intervertebral disc herniation, spinal stenosis	6

were injected once every three days for 60 days. At the end of each experiment (120 days), rats were euthanized for subsequent detection. The specific animal experimental scheme design is shown in (Supplementary Fig. 1).

2.4. Rat NP cell culture

All animal experimental procedures were approved by the Animal Care and Ethics Committee of Army Medical University. The rats were anesthetized with pentobarbital sodium (0.2%, 0.3 ml/100 g) and euthanized by cervical dislocation. And then, coccygeal IVDs were exposed to obtain NP tissues. Specifically, the tails of rats were routinely disinfected, the skin and subcutaneous tissues were incised along the posterior midline. The muscles, tendons and ligaments were bluntly separated with hemostatic forceps to expose IVDs. NP tissues were obtained through annulus fibrosus incision. 2 ml of type 2 collagenase (0.2%) was added, and the tissues were shaken gently, digested at 37 °C for 1–2 h, and then filtered through a 70-um filter. Rat NP cells were collected and planted in cells culture flasks in DMEM/F-12 (01-172-1ACS, BI, USA) containing 20% fetal bovine serum (S711–001 S, Lonsera, Uruguay), 100 units/mL penicillin and 100 ug/mL streptomycin (C0222, Beyotime, China) at 5% CO_2 and 37 °C. The NP cells were identified according to the previous studies (Supplementary Fig. 2) [23–25]. The second passage of NP cells were used for further experiments.

2.5. Treatment of NP cells

The Primary NP cells under 70–80% confluence was incubated in DMEM/F-12 containing the GANT61 (20uM, dissolved in DMSO) for 48 h at 5% CO_2 and 37 °C. Further, to determine the role of Fos inhibitor T5224 in Gli1 depletion NP cells. NP cells pretreated with GANT61 or Gli1 sh-RNA (sh-Gli1) were treated with T5224 (50uM, dissolved in DMSO) for 24 h, and cells were harvested for required experiments.

2.6. NP cells lentivirus transfection

To down-regulate Gli1 expression, lentivirus-coated sh-Gli1 were transfected into NP cells according to the previous protocol [26]. Lentivirus-coated empty vector was transfected into NP cells as negative control. The lentivirus vector was GV493, and the associated cis-acting element was hU6-MCS-CBh-gcGFP-IRES-puromycin. The sequences of sh-Gli1: Gli1-RNAi (98,828–1), TTGGATGAAGGACCTTGCGTT (The lentivirus and its vector were provided by Genechem, China). The transfected cells were cultured in DMEM/F-12 containing 2.5 ug/mL puromycin (ST551; Beyotime, China) for selection to obtain individual cell colony, and the expression of GFP protein in nucleus pulposus cells was observed by fluorescence microscopy (Olympus, Japan) to confirm the transfection efficiency. Further, western blot and RT-qPCR were used to verify whether sh-Gli1 was silenced successfully.

2.7. Western blot

Radioimmunoprecipitation assay lysis buffer (P0013, Beyotime) was added to collected tissues or cells to extract protein. The protein concentration was measured using a BCA protein assay kit (P0012, Beyotime, China). The protein samples were separated using SDS-PAGE and transferred to a 0.45-um PVDF membrane (Merck, Germany). Membranes were blocked by QuickBlock Western blocking solution (P0252, Beyotime, China) for 1 h and incubated with different kinds of primary antibodies (Table 1) at 4 °C overnight with rotation (the housekeeping proteins used in this study were GAPDH (whole protein/cytoplasmic protein) and Lamin B1 (nuclear protein)). TBST was used to wash off the unbound antibodies, and the membranes were incubated with the secondary antibodies of the corresponding species. secondary antibody was added, and the membrane was incubated for 1.5 h and washed again. Then, the membrane was covered with ECL working solution (1705062, Bio-Rad, USA) and incubated for 1–2 min. The membrane was placed in

the imaging system for imaging, and Image Lab software was used for analysis of the gray value.

2.8. Reverse transcription-quantitative PCR (RT-qPCR)

Total RNA was isolated from sh-Gli1 and sh-NC NP cells using 1 ml Trizol (9109, Takara Bio, Japan). RNA quality and quantity were determined using a NanoDrop ND-1000 spectrophotometer (Thermo Scientific, USA). One microgram RNA was reverse transcribed using a Prime Script RT Reagent kit (RR047A, Takara Bio, Japan) according to the manufacturer's protocols. Real-time quantitative PCR was performed in triplicate on a ViiA™ 7 Real-Time PCR system (Thermo Scientific, USA) with SYBR®Premix Ex Taq™ II (RR820A, Takara Bio, Japan). The 20 ul reaction mixtures (10 ul SYBR, 4 ul H_2O, 1 ul forward primer, 1 ul reverse primer and 4 ul cDNA) was amplified under the following conditions: 95 °C for 30 s, followed by 40 cycles of 95 °C for 5 s and 60 °C for 30 s. PCR products were subjected to melting curve analysis. Relative mRNA expression was calculated using the 2-ΔΔCt method. Lamin B1 was the internal reference gene. We measured the relative expression of Fos and Gli1 in NP cells. The primer sequences of the target genes are presented in Table 3.

2.9. Histological staining of rat IVD specimens

Rat coccygeal IVDs were decalcified for 14 days after fixation in 4% paraformaldehyde (PFA) solution. The samples were embedded in paraffin and sectioned into 5-mm-thick slices for histological staining or immunofluorescence (IF) as described below. To evaluate disc degeneration, the paraffinized slices were deparaffinized, hydrated, and subjected to hematoxylin and eosin (H&E) staining, safranin O staining to assess cellular and tissue morphology [27].

2.10. Immunofluorescence staining

Paraffin-embedded sections were placed in freshly prepared solution containing 3% hydrogen peroxide for 30 min, and then antigen repair was performed. The sections were deparaffinized with xylene and rehydrated with graded ethanol solutions, followed by antigen retrieval with sodium citrate-EDTA antigen retrieval solution (P0086, Beyotime, China). The sections were permeabilized, blocked, and incubated with primary antibodies (Table 1) overnight at 4 °C. Then, the sections were incubated with fluorescently labelled secondary antibodies (DyLight 488, 594) for 2 h in the dark at room temperature. The nuclei were counterstained with DAPI (C1002, Beyotime, China), and sections and cells were visualized using a fluorescence microscope (Lsm880, Zeiss, Germany).

2.11. Reactive oxygen species (ROS) measurement

ROS levels in NP cells were analyzed using the Cellular ROS Assay (deep red) (ab186029, Abcam, USA) and Reactive Oxygen Species Assay Kit (S0033, Beyotime, China). 200 ul of NP cells suspension (1–1.5 × 10^5) was incubated with 2 ul of Cellular ROS reaction mixture in 6-well microplate at 37 °C for 30 min in the dark. The observations were measured at 648 nm (ab186029) or 488 nm (S0033) using fluorescence microscope or flow cytometry.

Table 3
Primer sequence used in the RT-qPCR experiment.

S·NO.	Gene name	Primer sequence
1	Gli1	F-5′-AGCTGTGGGCATCCTGA-3′ R-5′-GGGGAGGGTACAAGGCA-3′
2	Fos	F-5′-CGAGGGGTTCCCGTAGA-3′ R-5′-ACTCCATGCGGTTGCTTT-3′
3	Lamin B1	F-5′-CCTTCTTCCCGAGTGACC-3′ R-5′-TCGCCTCTGATTCTTCCAC-3′

2.12. Mitochondrial membrane potential measurement

Mitochondrial membrane potential in NP cells were analyzed using the mitochondrial membrane potential assay kit with JC-1 (C2006, Beyotime, China). When the mitochondrial membrane potential is high, JC-1 aggregates in the matrix of the mitochondria, forming the aggregates (JC-1 aggregates), which produces red fluorescence. When the mitochondrial membrane potential is low, JC-1 cannot gather in the matrix of mitochondria, and then JC-1 is a monomer (JC-1 monomer), which produced green fluorescence. 200 ul of NP cells suspension (1–1.5 × 105) was incubated with 2 ul of mitochondrial membrane potential assay kit with JC-1 in 6-well microplate at 37 °C for 30 min in the dark. The observations were measured at 585/590 nm and 514/529 nm using fluorescence microscope.

2.13. Malondialdehyde (MDA), glutathione peroxidase (GPX) and superoxide dismutase (SOD) activity analysis

Total lipid peroxidation production , GPX and SOD activity were assessed by using MDA assay kit (S0131, Beyotime, China), glutathione peroxidase assay kit (S0058, Beyotime, China) and superoxide dismutase assay kit (S0101, Beyotime, China) respectively. NP cells or NP tissues were collected and lysed. The protein concentration of each sample was determined with a BCA kit. Then, 100 ul PBS was added to a centrifuge tube as a blank control, 100 ul standard of each concentration was used to generate a standard curve, and 100 ul sample solution was added for analysis. Each sample was analyzed in triplicate. Then, 100 ul corresponding detection solution and 100 ul supernatant were added to a 96-well plate, and the absorbance was determined with an ELISA plate reader. The contents and activity of MDA, GPX and SOD were calculated.

2.14. Apoptosis analysis

NP tissue: The IVDs sections were successively washed in xylene i 15min - xylene ii 15min absolute ethanol i 5min - absolute ethanol ii 5min-85% alcohol 5min-75% alcohol 5min-distilled water. After the sections were dry, an immunohistochemistry pen was used to draw a circle around the tissue, and 100ul of 1 × proteinase K working solution was added to the circle to cover the tissue, and the tissue was incubated at 37 °C for 20min. The glass slides were placed in PBS and washed on a decolorization shaker. Equilibration Buffer with 100ul TDT was added to each sample for 30min at 37 °C. Sections were placed in a humid box and incubated at 37 °C for 1 h with 50ul labelled working solution in the dark. Following washing, DAPI dye solution was incubated for 10 min. The sections were placed in PBS by shaking on a decolorization shaker. The slices were slightly dried and sealed with anti-fluorescence quenched tablet, and observed under a fluorescence microscope.

NP cells: The cell apoptosis was detected by One Step TUNEL Apoptosis Assay Kit (Beyotime, C1090, China) following the manufacturer's instructions. After incubated with the TUNEL regent in the dark for 30 min at 37 °C, cells were stained with DAPI. Apoptotic cells showed red fluorescence. Images of multiple cells from 3 independent experiments were obtained with a fluorescence microscope. In addition, we followed the previous method to detect apoptosis of NP cells by flow cytometry using Annexin V-PE/7AAD Kit (Solarbio, CA1030, China) [28].

2.15. Transmission electron microscopy (TEM)

The ultrastructure of NP cells was examined with TEM after sh-Gli1 lentivirus transfection group and then compared with the sh-NC

lentivirus transfection group. All cells were collected into a pellet and fixed with Electron microscopy fixation fluid (G1102, Service bio, China). The samples were then post-fixed for 2 h with 1% osmium tetroxide, followed by dehydration with graded ethanol. After infiltration and embedding with epon 812 (90,529-77-4, SPI, USA), the pellets were sliced into ultrathin sections (Leica UC7, Leica, Germany) and examined by transmission electron microscope (HT7700, Hitachi).

2.16. Magnetic resonance imaging (MRI)

Rats were anesthetized by inhalation of 4% sevoflurane (Obtained from Daping Hospital noninvasive Surgery Center, Chongqing, China). A magnetic resonance imager (Bruker Pharmascan 7.0 T, Germany) was used to scan the coccyx of the rats, and the parameters were set as follows: TR time: 3000 ms, TE time: 35 ms, incentive time: 7, scan time: 5 min 20 s, fat reduction technology: SPAIR, layer thickness: 0.8 mm, and spin echo sequence: TSE sequence. Pfirrmann grading of rat intervertebral discs was calculated according to the Pfirrmann grading criteria of T2-weighted imaging parameters [29]. The degree of IDD was determined in a double-blinded manner according to Pfirrmann classification and intervertebral height.

2.17. mRNA-seq analysis

Total RNA was extracted using Trizol reagent (15596018, Thermo Fisher, USA) following the manufacturer's procedure. The total RNA quantity and purity were analysis of Bioanalyzer 2100 and RNA 6000 Nano LabChip Kit (5067–1511, Agilent, usa), high-quality RNA samples with RIN number >7.0 were used to construct sequencing library. After total RNA was extracted, mRNA was purified from total RNA (5ug) using Dynabeads Oligo (dT) (Thermo Fisher, USA) with two rounds of purification. Following purification, the mRNA was fragmented into short fragments using divalent cations under elevated temperature (Magnesium RNA Fragmentation Module (cat. e6150, NEB, USA) under 94 °C 5–7min). Then the cleaved RNA fragments were reverse-transcribed to create the cDNA by SuperScript™ II Reverse Transcriptase (cat. 1896649, Invitrogen, USA), which were next used to synthesise U-labeled second-stranded DNAs with *E. coli* DNA polymerase I (cat. m0209, NEB, USA), RNase H (cat. m0297, NEB, USA) and dUTP Solution (cat. R0133, Thermo Fisher, USA). An A-base was then added to the blunt ends of each strand, preparing them for ligation to the indexed adapters. Each adapter contained a T-base overhang for ligating the adapter to the A-tailed fragmented DNA. Dual-index adapters were ligated to the fragments, and size selection was performed with AMPureXP beads. After the heat-labile UDG enzyme (cat. m0280, NEB, USA) treatment of the U-labeled second-stranded DNAs, the ligated products were amplified with PCR by the following conditions: initial denaturation at 95 °C for 3 min; 8 cycles of denaturation at 98 °C for 15 s, annealing at 60 °C for 15 s, and extension at 72 °C for 30 s; and then final extension at 72 °C for 5 min. The average insert size for the final cDNA librarys were 300 ± 50 bp. At last, we performed the 2 × 150bp paired-end sequencing (PE150) on an Illumina Novaseq™ 6000 (LC-Bio Technology CO., Ltd., China) following the vendor's recommended protocol. All processed and raw data were uploaded to GEO database under the Accession No. GSE217509 (https://www.ncbi.nlm.nih.gov/).

2.18. Statistical analyses

At least three biological replicates were used for all experiments. Normal distribution of the data was assessed using Shapiro–Wilk test. Non-normally distributed data is logarithmically converted to normally distributed data. Continuous data are presented as the mean ± SEM. Differences between two groups of normally distributed data were compared by Student's t test. Differences between groups were compared using one-way ANOVA. Statistical analysis was conducted with GraphPad and SPSS software. $P < 0.05$ was considered statistically significant.

3. Results

3.1. IDD with aging

Age is a major risk factor of IDD [30]. With age increasing, reticular NP cells change to chondrocyte-like nested NP cells. Meanwhile, there are significant changes in the structure of IVDs and the composition of NP [31]. In this study, we investigated the relationship between the degree of IDD and age in rats (2-month-old, 10-month-old and 20-month-old) and patients (youth group ≤35 years old, 35 years old < middle age group ≤65 years old, elderly group >65 years old; Table 2). MRI showed that the Pfirrmann grading of human IVDs was positively correlated with age. The T2 signal intensity of NP decreased with aging related IDD (Fig. 1A and B). Visual analogue scale (VAS) was used to evaluate the LBP of patients. It was found that the VAS score of the patients with Pfirrmann grading V was significantly higher than the patients with Pfirrmann grading II, and there is no significant difference between the VAS score of the patients with Pfirrmann grading III/IV and with Pfirrmann grading II (Fig. 1C). In addition, the Pfirrmann grading of rat IVDs was also positively correlated with aging (Fig. 1D and E). The NP area and intervertebral space height were negatively correlated with aging (Fig. 1F and G). H&E and safranin O staining of rat coccygeal IVDs showed the degenerative changes with aging (Fig. 1H and I). The ECM metabolism of NP tissues is crucial to IVD homeostasis [10]. The reduction of collagen II and ACAN is associated with IDD [32]. Consistently, with age increasing, the ECM catabolic enzyme MMP13 was increased significantly and the expression of ACAN and collagen II was decreased significantly in NP tissues (Fig. 1J and K).

3.2. Gli1 depletion, oxidative stress and apoptosis of NP cells in aging related IDD

The expression of Gli1 in human and rat NP tissues with different age was analyzed by IF staining and western blot. The results showed that the expression of Gli1, especially in the nucleus of NP cells, decreased with aging, suggesting that Gli1 in NP cells was depleted with the progression of IDD (Fig. 2A–E).

The homeostasis of the IVD changes significantly during IDD [32]. The oxidative stress and apoptosis in NP cells contribute to the disruption of IVD homeostasis [32,33]. SOD and GPX protect biological systems against the high chemical reactivity of reactive nitrogen species (RNS) or ROS during redox imbalance [34]. Enzyme activity analysis showed that the activity of GPX and SOD was decreased in aging related IDD (Fig. 3A). Western blot showed that the expression of GPX4 and SOD2 was also decreased with rat and human IDD progression (Fig. 3C–F). 4HNE and MDA, lipid peroxidation metabolic products, are biomarkers of oxidative stress [35]. It showed that 4HNE and MDA were increased with IDD progression (Fig. 3B–F). ROS level in NP cells from 2-month-old rats and 20-month-old rats were analyzed. It was found that ROS level increased significantly with aging (Supplementary Fig. 3A). Moreover, TUNEL staining and flow cytometry were used to investigate the apoptosis of NP cells during IDD. The results showed that the apoptotic rate of NP cells increased significantly with aging (Fig. 3G, Supplementary Fig. 3B). Western blot demonstrated that the expression of cleaved caspase3 and Bax in NP tissues was significantly increased with aging (Fig. 3H–K). These results indicated that the enhanced oxidative stress and increased apoptosis of NP cells during aging related IDD.

3.3. Gli1 depletion induced oxidative stress and apoptosis of NP cells

To elucidate the effect of Gli1 depletion on the oxidative stress and apoptosis of NP cells, lentivirus-coated sh-Gli1 and the Gli1-targeting inhibitor GANT61 were used to inhibit Gli1 expression in NP cells (Fig. 4A). The morphology of sh-Gli1-infected and sh–NC–infected NP cells were compared by TEM. The cellular morphology and nucleus of NP cells treated with sh-Gli1 were irregular, and the nucleoli were

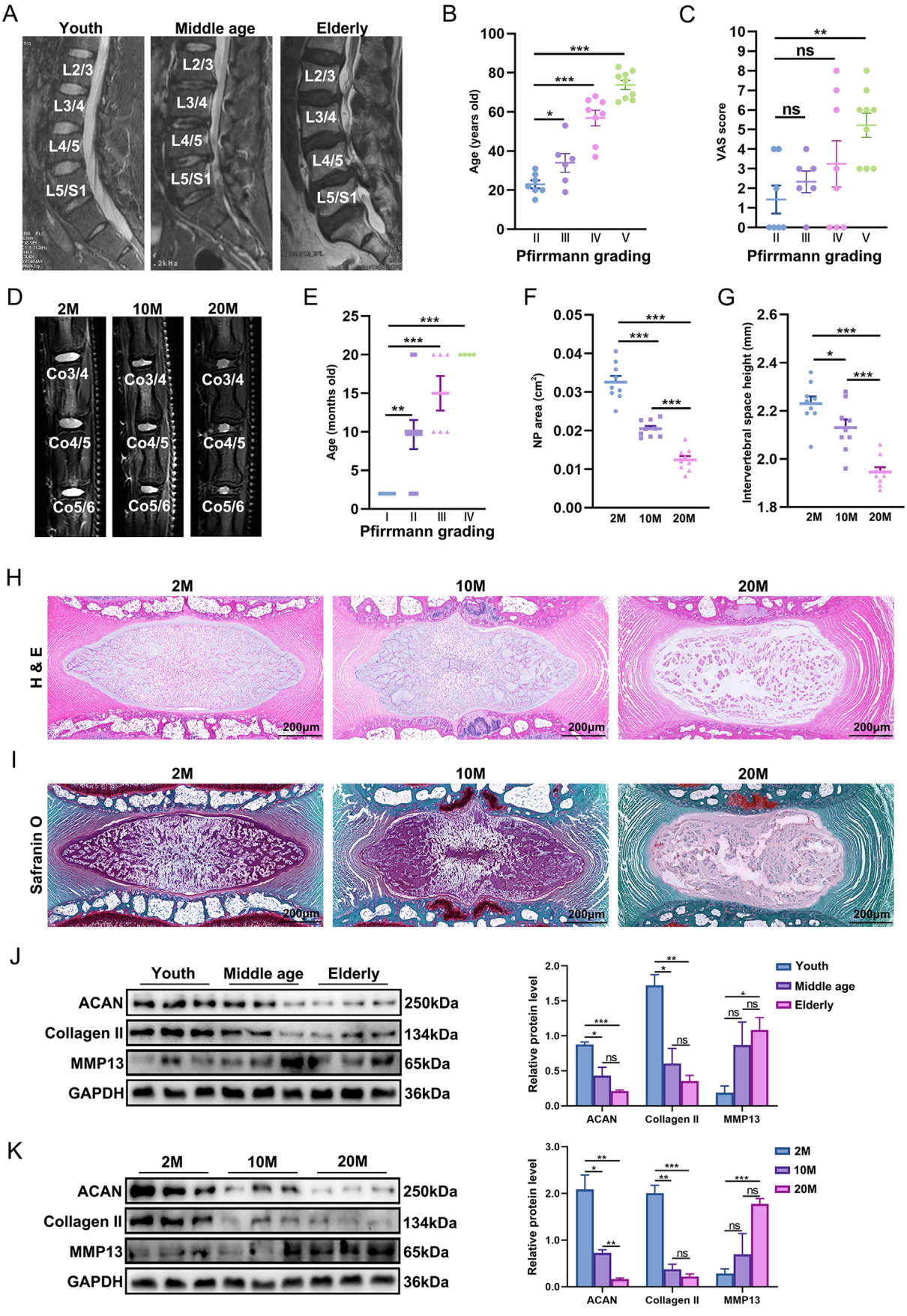

(caption on next page)

Fig. 1. The IDD with aging (A, B) Representative MRI imaging and Pfirrmann grading of human lumbar IVDs at different ages. Youth group (<35 years old, n = 10), Middle age group (35–65 years old, n = 10), Elderly (>65 years old, n = 10) (C) Lumbar VAS score from patients at different Pfirrmann grading (D–G) MRI of rat coccygeal IVDs at different ages. Measurement of Pfirrmann grading, NP tissue area and intervertebral space height (n = 3, 3 IVDs were detected in each rat, and a total of 9 IVDs were counted) (H, I) H&E and safranine O staining of rat coccygeal IVD sections at different ages (J) Western blot and quantification of ACAN, collagen II and MMP13 in human NP tissues at different ages (n = 3) (K) Western blot and quantification of ACAN, collagen II and MMP13 in rats NP tissue at different ages (n = 3). The data are expressed as the mean ± SEM, * = $p < 0.05$, ** = $p < 0.01$, *** = $p < 0.001$, ns = no statistical significance. Abbreviations: 2 M: 2-month-old; 10 M: 10-month-old; 20 M: 20-month-old.

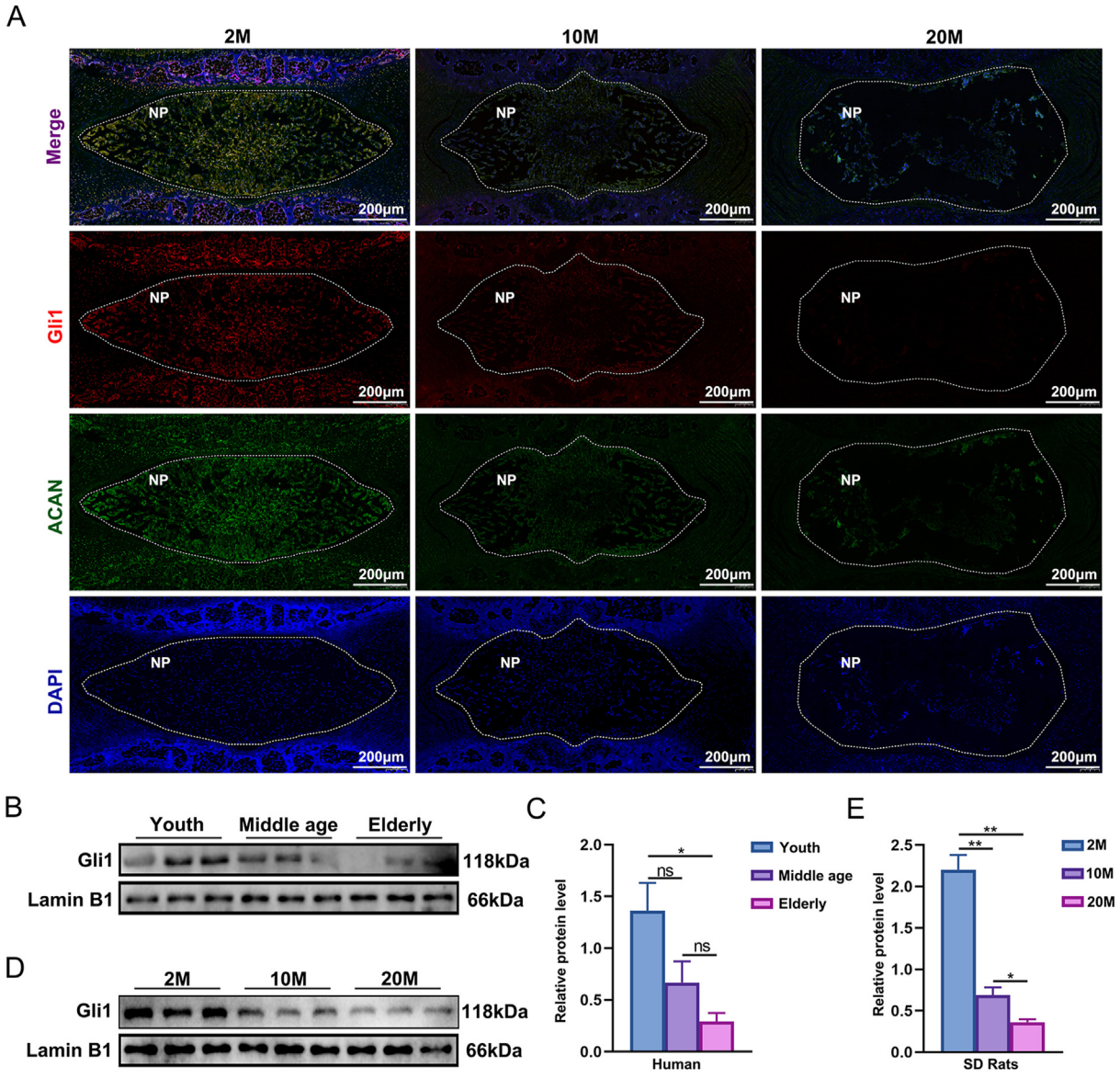

Fig. 2. Gli1 depletion of NP cells in aging related IDD (A) Immunofluorescence staining of Gli1 and ACAN in the coccygeal IVDs of rats at different ages (B, C) Western blot and quantification of Gli1 in human NP tissue at different ages (n = 3) (D, E) Western blot and quantification of Gli1 in rats NP tissue at different ages (n = 3). The data are expressed as the mean ± SEM, * = $p < 0.05$, ** = $p < 0.01$, *** = $p < 0.001$, ns = no statistical significance. Abbreviations: 2 M: 2-month-old; 10 M: 10-month-old; 20 M: 20-month-old.

disassembled. The number of mitochondria decreased and their morphology was swollen. The mitochondrial matrix became shallow and uneven, and the mitochondrial cristae became short or absent. The rough endoplasmic reticulum was dilated and degranulated. A small number of autolysosomes were found in cells. In contrast, the cellular morphology of NP cells treated with sh-NC was oval with a uniform cytoplasm and intact cell membrane. The shape of nucleus was irregular and the chromatins were evenly distributed without pyknosis, and the nucleoli were obvious. Mitochondria cristae were arranged neatly. The rough endoplasmic reticulum was abundant. The Golgi apparatus showed no hypertrophy or hyperplasia (Fig. 4B). The production of ROS in Gli1 depleted NP cells was higher than that in the control (Fig. 4C–D). The expression of GPX4 and SOD2 were significantly decreased, while the expression of 4HNE was increased in Gli1 depleted NP cells (Fig. 4E and F). Consistently, the activity of GPX and SOD was significantly reduced, and the level of MDA was significantly increased (Fig. 4G and H). Mitochondrial dysfunction is also important sources of oxidative stress. We examined the effect of Gli1 depletion on the mitochondrial

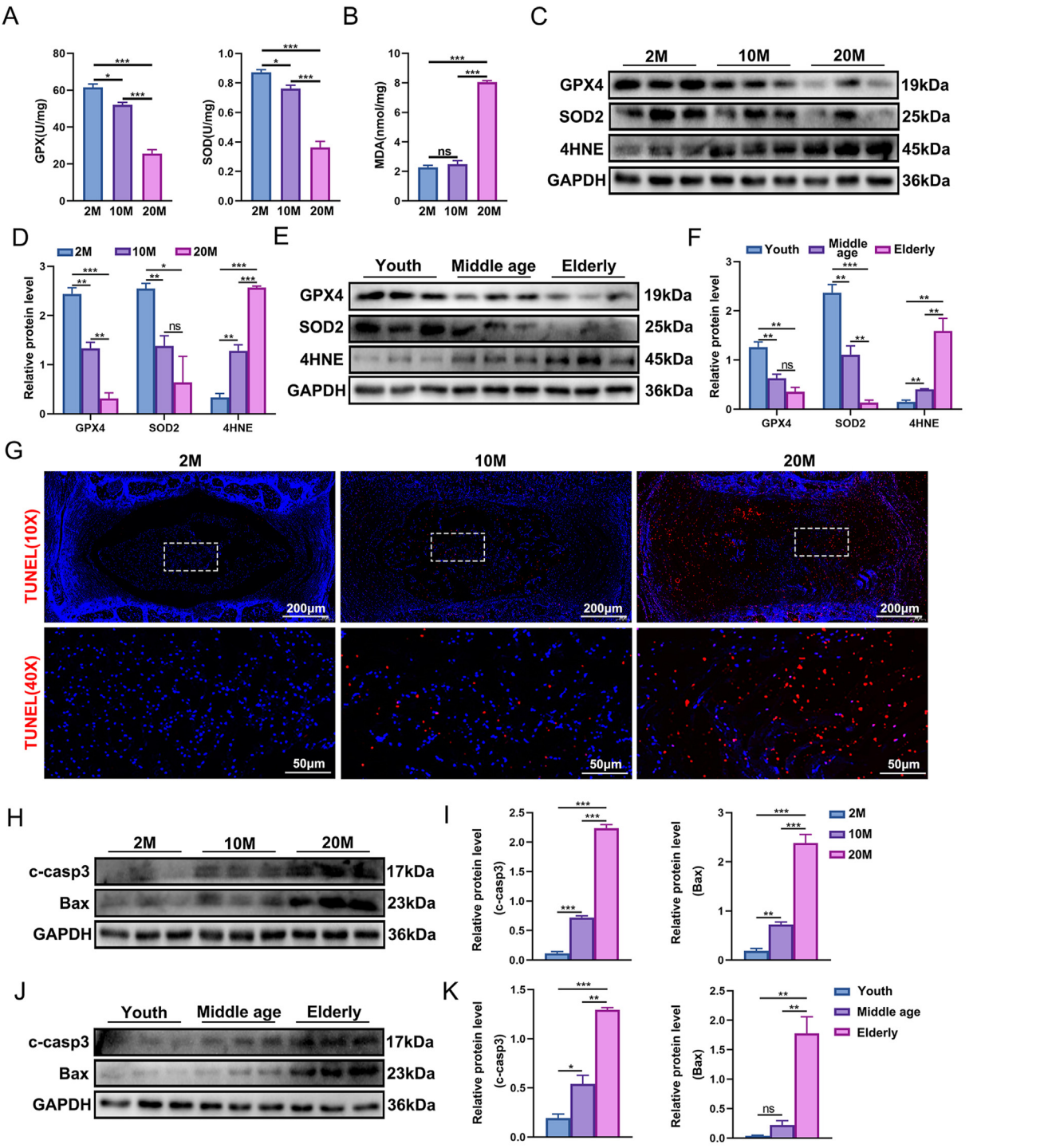

Fig. 3. Oxidative stress and apoptosis of NP cells in aging related IDD (A) GPX and SOD enzyme activity in rat coccygeal NP tissues at different ages (n = 3) (B) MDA accumulation level in rat coccygeal NP tissues at different ages (n = 3) (C, D) Western blot and quantification of GPX4, SOD2 and 4HNE in rats NP tissue at different ages (n = 3) (E, F) Western blot and quantification of GPX4, SOD2 and 4HNE in human NP tissue at different ages (n = 3) (G) TUNEL staining of coccygeal IVDs from rats at different ages (H, I) Western blot and quantification of c-casp3 and Bax in rats NP tissue at different ages (n = 3) (J, K) Western blot and quantification of c-casp3 and Bax in human NP tissue at different ages (n = 3). Statistical data are expressed as the mean ± SEM, * = $p < 0.05$, ** = $p < 0.01$, *** = $p < 0.001$, ns = no statistical significance. Abbreviations: 2 M: 2-month-old; 10 M: 10-month-old; 20 M: 20-month-old.

membrane potential of NP cells. We found that GANT61 decreased JC-1 aggregates and increased JC-1 monomer, indicating the decreased mitochondrial membrane potential of NP cells. It suggested that mitochondrial dysfunction in NP cells is induced by Gli1 depletion (Supplementary Fig. 4). TUNEL staining showed that Gli1 depletion resulted in an enhanced NP cell apoptosis (Fig. 4I and J). Western blot showed that Gli1 depletion significantly increased the expression of cleaved caspase 3 and Bax (Fig. 4K and L).

3.4. Gli1 depletion caused Fos activation in NP cells

The differentially expressed genes (DEGs) in NP cells treated with

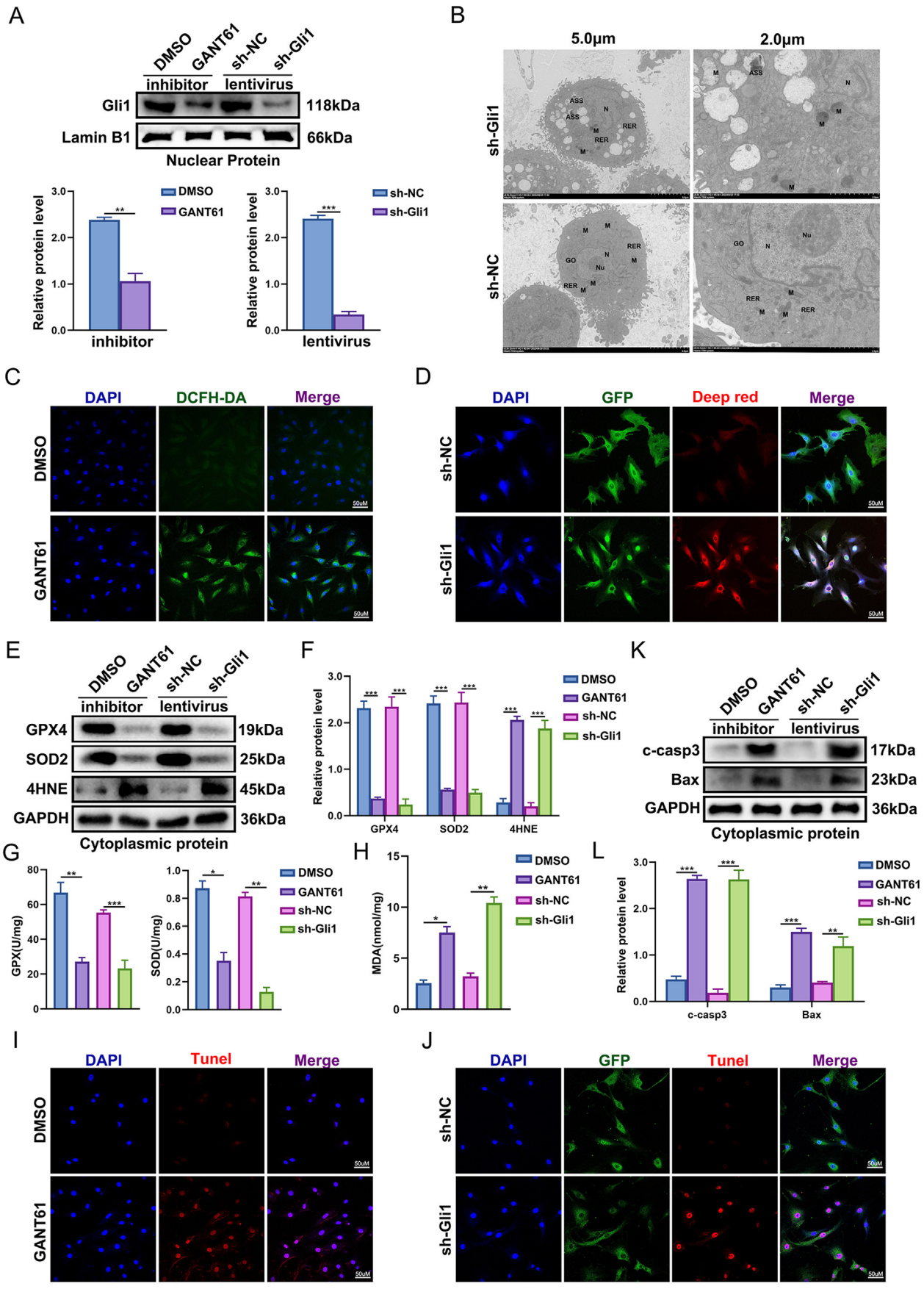

(caption on next page)

Fig. 4. Gli1 depletion induced oxidative stress and apoptosis of NP cells (A) Western blot and quantification of Gli1 in NP cells treated with different agents (n = 3) (B) The morphology of NP cells treated with sh-Gli1 and sh-NC was observed by TEM (C) ROS measurement by DCFH-DA of rat NP cells treated with DMSO and GANT61 (D) ROS measurement by Deep red of rat NP cells treated with sh-NC and sh-Gli1 (GFP is the native luminescent protein of lentiviral vector) (E, F) Western blot and quantification of GPX4, SOD2 and 4HNE in NP cells treated with different agents (n = 3) (G) GPX and SOD enzymes activity in NP cells treated with different agents (n = 3) (H) MDA accumulation level in NP cells treated with different agents (n = 3) (I) TUNEL staining of rat NP cells treated with DMSO and GANT61 (J) TUNEL staining of rat NP cells treated with sh-NC and sh-Gli1 (GFP is the native luminescent protein of lentiviral vector) (K, L) Western blot and quantification of c-casp3 and Bax in NP cells treated with different agents (n = 3). The data are expressed as the mean ± SEM, * = $p < 0.05$, ** = $p < 0.01$, *** = $p < 0.001$, ns = no statistical significance. Abbreviations: nucleus: N; nucleoli: Nu; mitochondria: M; rough endoplasmic reticulum: RER; golgi apparatus: GO; autolysosomes: ASS. (For interpretation of the references to colour in this figure legend, the reader is referred to the Web version of this article.)

lentivirus-coated sh-Gli1 groups (n = 3) were analyzed by mRNA-seq. As shown in the volcano plot, among the DEGs, 943 were significantly downregulated and 2655 genes were significantly upregulated (Fig. 5A). Gene ontogeny (GO) analysis showed that the apoptosis-related and oxidation-reduction biological functions were significantly enriched by DEGs (Fig. 5B). Based on Kyoto Encyclopedia of Genes and Genomes (KEGG) analysis, the apoptosis pathway was also found to be enriched by DEGs (Fig. 5C). Furthermore, gene set enrichment analysis (GSEA) showed that the sh-Gli1-treated NP cells were characterized by an enrichment of apoptosis-related genes (Fig. 5D). The genes associated with the apoptosis pathway were showed as heatmap. It shows that 25 genes were significantly increased in the sh-Gli1 treatment group, among which the Fos showing the most notable increase (Fig. 5E). This change in NP cells was confirmed by qRT-PCR and western blot further (Fig. 5F and G). We analyzed the GSE100936 in the GEO database of NCBI and found that for Gli1 peak regions with Gli1-consensus binding motifs in humans and rats, significant enrichment was found for Fos ($p < 1e^{-5}$) motifs. These results indicated that Fos may mediate the NP cell apoptosis induced by Gli1 depletion.

3.5. Fos suppression retarded oxidative stress and apoptosis in Gli1 depleted NP cells

To further verify the roles of Fos in the oxidative stress and apoptosis of NP cells induced by Gli1 depletion, Fos specific inhibitor, T5224, was used to suppress Fos activation in NP cells. Western blot demonstrated that T5224 significantly impeded the up-regulation of Fos induced by GANT61 or sh-Gli1 (Fig. 6A). Fig. 6B and C showed that T5224 significantly increased the expression of GPX4 and SOD2 and enzyme activity of GPX and SOD in the Gli1 depleted NP cells. On the other hand, the up-regulation of MDA caused by Gli1 depletion was inhibited by T5224 effectively (Fig. 6D). Fluorescence microscopy showed that T5224 treatment partially relieved the effect of Gli1 depletion on ROS accumulation in NP cells (Fig. 6E and F). Besides, T5224 significantly alleviated NP cell apoptosis induced by Gli1 depletion (Fig. 6G–I).

3.6. Fos suppression ameliorated exogenous Gli1 depletion induced IDD

Since Fos suppression retarded the pro-apoptotic effect of Gli1 depletion on NP cells, we tried to find out whether Fos suppression can ameliorated IDD induced by Gli1 depletion. Intraperitoneal injection of GANT61 exogenously leaded to the down-regulation of Gli1 in rat NP tissues (Fig. 7G, Supplementary Fig. 5), and promoted IDD. Specifically, GANT61 decreased the NP area, the intervertebral space height and the expression of ACAN and collagen II in NP tissues. Meanwhile, the Pfirrmann grading and the expression of MMP13 in NP tissues were increased by GANT61. These changes were alleviated by Fos suppression caused by intraperitoneal injection of T5224 (Fig. 7A, B, G, Supplementary Fig. 5). H&E and safranin O staining of IVDs were shown in Fig. 7C indicated GANT61 treatment caused a decrease in the number of NP cells, ECM fibrosis and the disorders of annulus fibrosus structure, which was retarded by intraperitoneal injection of T5224. It suggested that Fos suppression ameliorated exogenous Gli1 depletion induced IDD. Also, exogenous Gli1 depletion inhibited the expression of GPX4 and SOD2, as well as the activity of GPX and SOD and increased the accumulation of MDA and 4HNE in NP tissues. Fos suppression has significantly alleviated the increasing of oxidative stress (Fig. 7D, E, G, Supplementary Fig. 5). For apoptosis, exogenous Gli1 depletion resulted in an increased TUNEL staining and an up-regulation of Bax and c-caspse3, which was alleviated by Fos suppression (Fig. 7F and G, Supplementary Fig. 5). These evidences suggested that Fos suppression ameliorated exogenous Gli1 depletion induced oxidative stress and apoptosis of NP cells as well as IDD.

4. Discussion

The treatment and prevention of IDD are still affected by phenotype and fate of NP cells [36,37]. In particular, the affection of the IVD homeostasis by aging remains unknown. In this study, we focused on Gli1, the most critical transcription factor associated with IVD development and structural maintenance, and investigated the role of Gli1 in the pathogenesis of IDD. The results showed that Gli1 was depleted accompanied by the enhanced oxidative stress and increased apoptosis of NP cells in aging related IDD. Also, we found that Gli1 depletion indued NP cell oxidative stress, NP cell apoptosis and IDD via Fos activation. In conclusion, our study highlights the crucial role of Gli1 depletion in the regulation of oxidative stress and apoptosis in NP cells and provide a novel insight into the pathogenesis of IDD. Fos is a promising target for the prevention and treatment of IDD. In addition, this study provides a new perspective on the precise regulation of oxidative stress and apoptosis in NP cells.

In 1995, Buckwalter carried out a pioneering systematic study on the relationship between IDD and age in human and found that the structure, biochemistry and biodynamics of IVDs change with aging. Consequently, IVDs become degenerative [38]. Michal et al. indicated that IVDs have an intrinsic circadian clock that is regulated by age and is associated with IDD [39]. Recently, researchers have begun to use animal models to study the pathogenesis of aging related IDD. Matthew A et al. conducted the transcriptome analysis of mouse IVDs at different ages. Sarthak Mohanty et al. reported the phenotypic change of mouse NP cells with aging [31,40]. In the current study, we found that with aging, rat NP tissues gradually shrank and lost their elasticity. Anulus fibrosus (AF) gradually thickened and became disordered, and the boundary between the AF and NP gradually became blurred. The MRI-T2 signal intensity, area of the NP and height of the intervertebral space decreased. The vacuolated and reticular-shaped NP cells were transformed into chondrocyte-like nested NP cells. The number of NP cells gradually decreased. The number of cracks between cells increased, and the cells were surrounded by more ECM. These results indicate that the aging related IDD of rats is a reliable research model.

The Shh pathway is closely related to growth and development. Choi et al. found that during embryonic development, the Shh pathway plays a key role in the morphogenesis of NP, IVDs and spine by regulating notochord cell proliferation and migration [41,42]. Dahia et al. found that during the neonatal period, the Shh pathway is still activated in the NP of mice. Knockout of Shh gene or pharmacological inhibition of Shh pathway result in loss of the differentiated phenotype of NP, AF and cartilage endplate cells, disorder of NP reticular structure, AF collagen structure and disc collapse [16,43]. A previous study also found that inhibition of Shh pathway is closely related to sacral disc collapse and

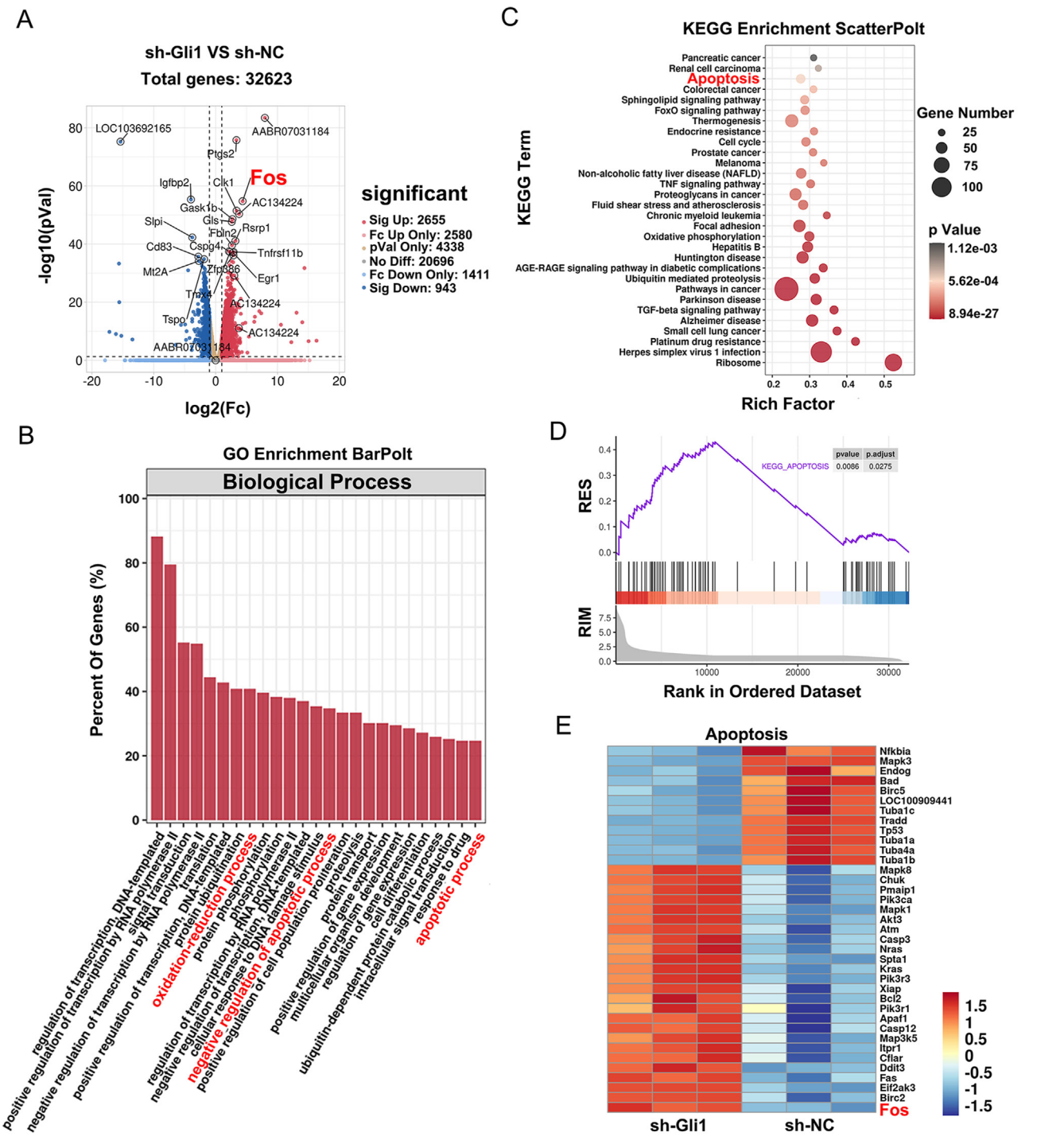

(caption on next page)

Fig. 5. Fos activation caused by Gli1 depletion in NP cells (A) Volcano plot of differentially expressed genes between sh-Gli1 and sh-NC NP cells (n = 3). Fold-change (x-axis) is plotted against statistical significance (y-axis) for each gene set. Genes significantly upregulated are located within the red quadrants, and those significantly downregulated are located within the blue quadrants based on a threshold of fold-change ≥2 and $p < 0.05$ (number of significantly altered genes is indicated in each of the quadrants). The ten most differentially expressed genes in each quadrant are indicated by their gene symbols on the plots (arrows) (B, C) GO and KEGG enrichment analyses of differentially expressed genes (D) GSEA showed that sh-Gli1 NP cells were characterized by an enrichment of apoptosis-related genes (E) Heatmap of differentially expressed genes that were enriched in apoptosis pathways (F) qRT-PCR of Gli1 and Fos in sh-Gli1 and sh-NC NP cells (n = 3) (G) Western blot and quantification of Gli1 and Fos in sh-Gli1 and sh-NC NP cells (n = 3). The data are expressed as the mean ± SEM, * = $p < 0.05$, ** = $p < 0.01$, *** = $p < 0.001$, ns = no statistical significance. (For interpretation of the references to colour in this figure legend, the reader is referred to the Web version of this article.)

sacral fusion, demonstrating that Shh pathway plays an essential role in disc growth and differentiation [44]. Gli1, a key transcriptional factor of the Shh pathway, has been proposed as a major effector protein. However, the role of Gli1 in the maintenance of IVD homeostasis is still unclear. Based on the NP tissue of human and rat, we found that Gli1 was gradually depleted in degenerative IVDs, which was consistent with the previous study that demonstrated the gradually decreased expression of Gli1 in aging mouse NP [40]. However, the role of Gli1 in IVD homeostasis and the underlying molecular mechanism have rarely been studied. To assess the effect of Gli1 on the maintenance of IVD homeostasis, we administered GANT61 by intraperitoneal injection to suppress the expression of Gli1 in rat caudal IVDs. Histological and imaging evidences showed that exogenous Gli1 depletion accelerated IDD progression. These results indicate that Gli1 not only plays an important role in IVD generation and development in the prenatal and neonatal periods, but also plays an important role in IVD homeostasis maintenance after birth.

The significant decrease in the proportion of Gli1-positive NP cells suggested that IVD homeostasis was more vulnerable during IDD. This phenomenon was consistent with other types of degenerative diseases, such as neurodegenerative diseases [21,45]. Mechanistically, these NP cells were functional in adulthood. The DNA of NP cells was exposed to oxidative stress and the exhibited impaired antioxidant protection, leading the NP cells more susceptible to death and reducing the number of functional NP cells [46,47]. This theory led us to evaluate the involvement of Gli1 depletion in the oxidative stress and apoptosis of NP cells. The accumulation of intracellular ROS caused by the imbalance of the oxygen free radical metabolism system was the main cause of oxidative stress in NP cells [11,48]. Oxidative stress leads to NP cell apoptosis and destroyed the structural and functional homeostasis of IVDs by regulating apoptosis [49,50]. Based on the aging related IDD of SD rats, we found that the oxidative stress and apoptosis of NP cell were dramatically increased. Concordantly, we found induction of oxidative stress promoted NP cell apoptosis. Noticeably, several studies have reported that the Shh signaling pathway protects cells from oxidative stress and regulated the occurrence, treatment and prevention of degenerative diseases [51–53]. As the most important transcription factor of the Shh signaling pathway, Gli1 played a key role in this process [54]. In a mouse renal ischemia/reperfusion injury model and mouse colitis model, Gli1-mediated polydatin inhibited cell apoptosis by suppressing oxidative, and consequently attenuated renal ischemia/reperfusion injury and colitis [19,55]. In endometrial hyperplasia, Gli1 activation repressed oxidative stress by protecting mitochondrial function and maintaining mitochondrial membrane potential [20]. Herein, to elucidate the effects of Gli1 on the oxidative stress and apoptosis, GANT61 and lentivirus-coated sh-Gli1 were used to induce the Gli1 depletion of NP cells at the protein level and transcription level respectively, which are beneficial to acquiring more reasonable and rigorous results. Consistent with the previous reports, Gli1 depletion significantly reduced mitochondrial membrane potential, and resulted in mitochondrial dysfunction and oxidative stress in NP cells. Consequently, the apoptosis of NP cells was significantly increased. Gli1 depletion is an essential contributor for the oxidative stress and apoptosis of NP cells in degenerative IVDs.

Based on the results of mRNA-seq, Fos, Fas, Casp3, Casp12, MAPK family genes and other apoptotic genes were main DEGs after Gli1 depletion. Fos was the most significantly altered among the DEGs. As a subunit of the transcription factor activator protein 1 (AP-1), Fos is involved in a variety of biological processes and plays important roles in various tissue types [56,57]. Previous studies have reported that Fos is a key pro-apoptotic gene, and Fos suppression effectively retarded cell apoptosis [58,59]. Recently, AP-1/Fos suppression has been shown to suppress cellular oxidative stress by up-regulating the expression of antioxidants [60]. Ishihara, Y. et al. demonstrated that oxidative stress increased Fos expression and led to hepatocyte apoptosis [61]. In 2019, Shabana Amanda Ali et al. identified Gli1 binding sites in the conserved Fos region by Gli1 chip-seq analysis of human chondrosarcoma [62]. Therefore, we investigated the roles of Fos in the oxidative stress and apoptosis of NP cells induced by Gli1 depletion. The results showed that Fos inhibitor T5224 prominently retarded the oxidative stress and apoptosis of NP cells caused by Gli1 depletion, indicating that Fos mediates the pro-oxidative and pro-apoptotic effects of Gli1 depletion on NP cells.

The effect of Gli1 depletion on IVD homeostasis, and the role of Fos in exogenous Gli1 depletion induced IDD were analyzed in vivo. Intraperitoneal injection of GANT61 effectively down-regulated Gli1 expression and up-regulated Fos expression in rat NP tissues. The imaging and histological analysis demonstrated rat IDD indued by exogenous Gli1 depletion. Consistent with the in vitro experiments, mainly characterized by the decrease of NP water content, AF gradually thickened and became disordered, the boundary between NP and AF gradually blurred, the vacuolated and reticular-shaped NP cells were transformed into chondrocyte-like nested NP cells, the number of NP cells decreased gradually, the intercellular cleft increased, the ECM increased, and the NP area and intervertebral space height decreased. Moreover, intraperitoneal injection of GANT61 also resulted in oxidative stress and NP cell apoptosis. Furthermore, T5224 was injected intraperitoneally to suppress Fos expression in rat NP tissues. As a result, the exogenous Gli1 depletion induced IDD was significantly ameliorated. Likewise, intraperitoneal injection of T5224 dramatically alleviated the oxidative stress and apoptosis caused by exogenous Gli1 depletion. Fos is a potential therapeutic target of IDD.

There were several limitations in the current study. We cannot ignore the fact that rat and human have different spinal biomechanical properties. In addition, Gli1 depletion by exogenous GANT61 does not necessarily have the same effects as the induction of endogenous aging related Gli1 depletion. In the future, we will construct C57 mice with conditional Gli1 knockout. It would be more scientific to investigate the effects of Gli1 depletion and interfering measures on IVDs based on this model. Lastly, the intraperitoneal injection of drugs affects other organs inevitably and exert both direct and indirect effects on IVDs, which causes some biases.

In conclusion, our study revealed that Gli1 depletion in IVDs stimulates oxidative stress in NP cells and causes NP cell apoptosis by activating Fos, which consequently disturbs the homeostasis of IVDs and leads to IDD. These findings highlight a beneficial role of Gli1 in IVD homeostasis maintenance and IVD regeneration. Marinating Gli1 expression and suppressing Fos activation in NP cells are promising targets for the prevention and treatment of IDD.

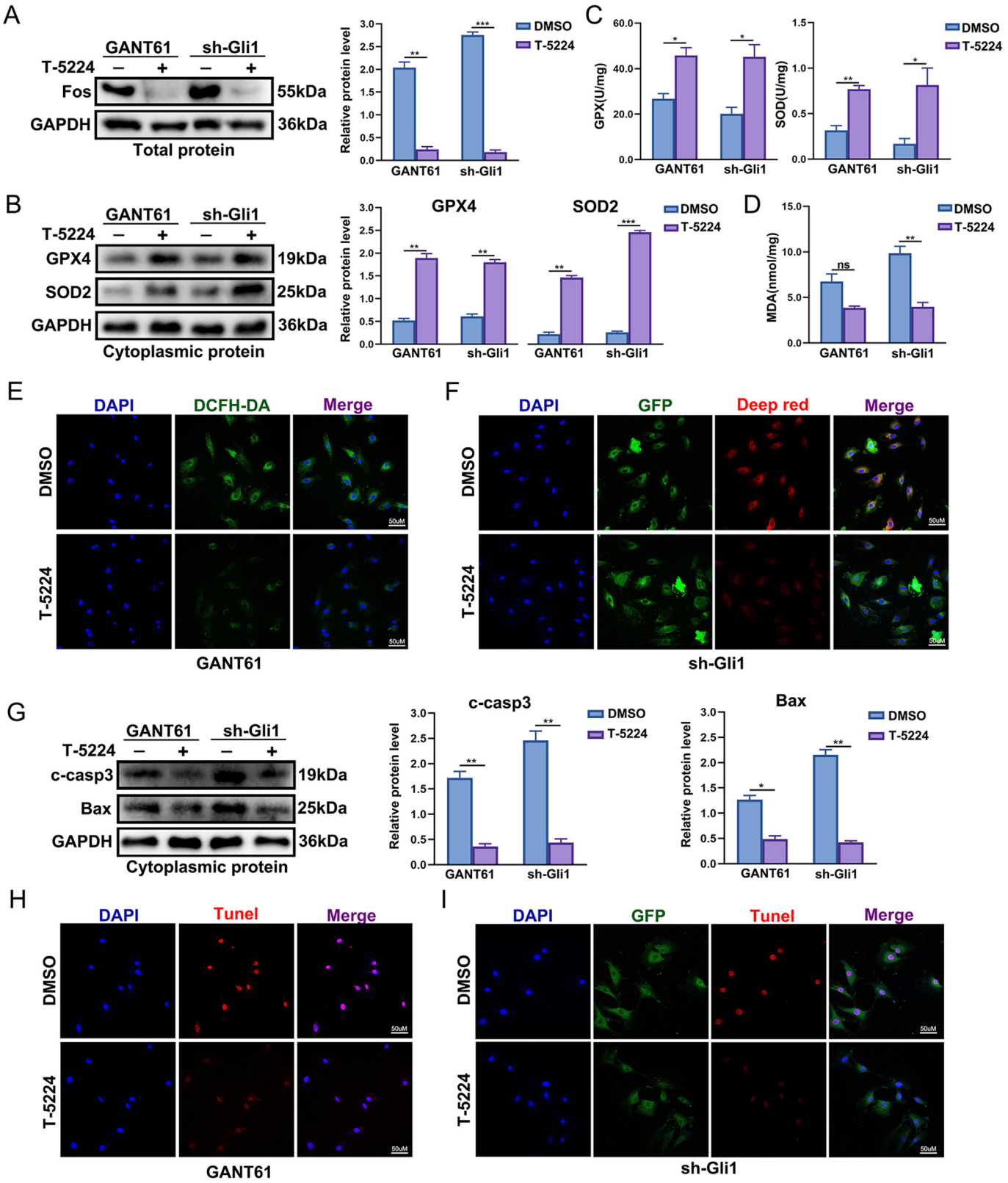

Fig. 6. Fos suppression suppressed the oxidative stress and apoptosis of Gli1 depleted NP cells (A) Western blot and quantification of Fos in NP cells treated with different agents (n = 3) (B) Western blot and quantification of GPX4 and SOD2 in NP cells treated with different agents (n = 3) (C) GPX and SOD enzymes activity in NP cells treated with different agents (n = 3) (D) MDA accumulation level in NP cells treated with different agents (n = 3) (E) ROS measurement by DCFH-DA of rat NP cells treated with different agents (F) ROS measurement by Deep red of rat NP cells treated with different agents (GFP is the native luminescent protein of lentiviral vector) (G) Western blot and quantification of c-casp3 and Bax in NP cells treated with different agents (n = 3) (H) TUNEL staining of rat NP cells treated with different agents (I) TUNEL staining of rat NP cells treated with different agents (GFP is the native luminescent protein of lentiviral vector). The data are expressed as the mean ± SEM, * = $p < 0.05$, ** = $p < 0.01$, *** = $p < 0.001$, ns = no statistical significance. (For interpretation of the references to colour in this figure legend, the reader is referred to the Web version of this article.)

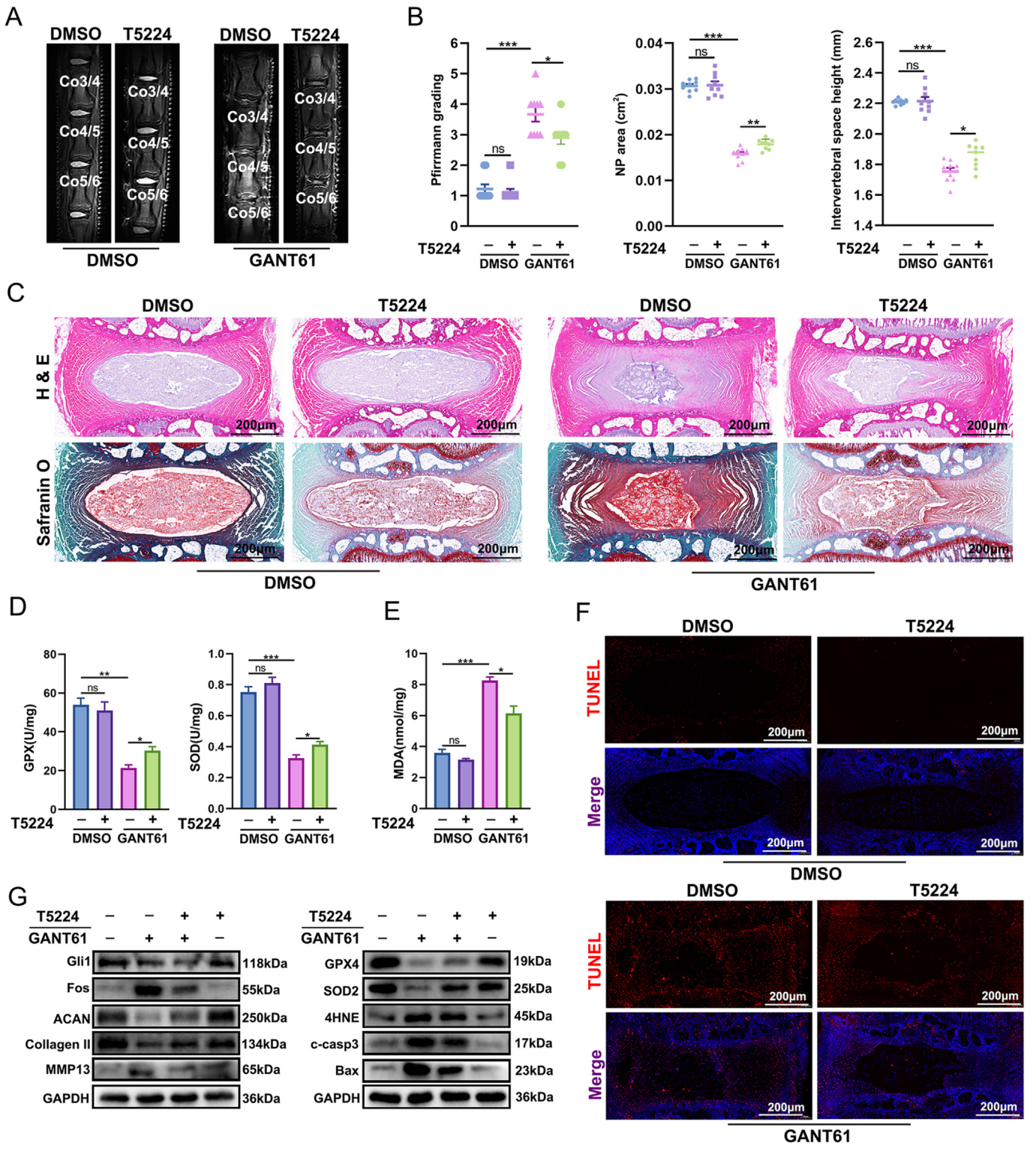

Fig. 7. Fos suppression alleviated exogenous Gli1 depletion induced IDD (A, B) MRI of rat coccygeal IVDs treated with different agents. Measurement of Pfirrmann grading, NP tissue area and intervertebral space height (n = 3, 3 IVDs were detected in each rat, and a total of 9 IVDs were counted) (C) H&E and safranine O staining of rat coccygeal IVD sections treated with different agents (D) GPX and SOD enzymes activity of NP tissue treated with different agents (n = 3) (E) MDA accumulation level of NP tissue treated with different agents (n = 3) (F) TUNEL staining of coccygeal IVDs treated with different agents (G) Western blot and quantification of Gli1, Fos, ACAN, collagen II, MMP13, GPX4, SOD2, 4HNE, c-casp3 and Bax of NP tissue in rats treated with different agents (n = 3). The data are expressed as the mean ± SEM, * = $p < 0.05$, ** = $p < 0.01$, *** = $p < 0.001$, ns = no statistical significance.

Authors' contributions

FCC, ZY, and LCQ conceived and designed the experiments; LLBX and ZYY performed the experiments; LLBX, AXZ and FJW participated in the creation of the experimental animal model. FJW and FCC revised the article and conducted the experiments complementation; LX and ZY analysed the data; LLBX and ZYY edited the figures and wrote this article; FCC reviewed the article and polished the language. All authors read and approved the final manuscript.

Funding

This work was supported by National Natural Science Foundation of China, China (grant number 81902255, 82072495), Natural Science Foundation of Chongqing, China (grant number cstc2020jcyj-bshX0091), China Postdoctoral Science Foundation, China (grant number 2020M673652), Discipline Innovation Project of Army Military Medical University Xinqiao hospital (grant number 310910SZXK), Special Foundation of Army Military Medical University to enhance scientific and technological innovation ability (grant number 2020XQN15), Chongqing Postdoctoral Program Special funding (grant number 2021XM3016).

Data availability statement

The data that support the findings of this study are available from the corresponding author upon reasonable request. Transcriptome analysis and sequencing raw data have been stored in the Gene Expression Omnibus (GEO) database (https://www.ncbi.nlm.nih.gov/). GSE217509 (Effect of depletion of Gli1 on gene expression of primary rat nucleus pulposus cells).

Declaration of competing interest

The authors declare that they have no conflicting interests.

Appendix A. Supplementary data

Supplementary data related to this article can be found at https://doi.org/10.1016/j.jot.2023.05.008.

References

[1] Global burden of 369 diseases and injuries in 204 countries and territories, 1990-2019: a systematic analysis for the Global Burden of Disease Study 2019. Lancet (London, England) 2020;396(10258):1204–22.
[2] Jin Z, Wang D, Zhang H, Liang J, Feng X, Zhao. J. , et al. Incidence trend of five common musculoskeletal disorders from 1990 to 2017 at the global, regional and national level: results from the global burden of disease study 2017. Ann Rheum Dis 2020;79(8):1014–22.
[3] Stevans JM, Delitto A, Khoja SS, Patterson CG, Smith CN, Schneider MJ, et al. Risk factors associated with transition from acute to chronic low back pain in US patients seeking primary Care. JAMA Netw Open 2021;4(2):e2037371.
[4] Vlaeyen JWS, Maher CG, Wiech K, Van Zundert J, Meloto CB, Diatchenko L, et al. Low back pain. Nat Rev Dis Prim 2018;4(1):52.
[5] Livshits G, Popham M, Malkin I, Sambrook PN, Macgregor AJ. Spector, T.,et al. Lumbar disc degeneration and genetic factors are the main risk factors for low back pain in women: the UK Twin Spine Study. Ann Rheum Dis 2011;70(10):1740–5.
[6] Lyu F-J, Cheung KM, Zheng Z, Wang H, Sakai D, Leung VY. IVD progenitor cells: a new horizon for understanding disc homeostasis and repair. Nat Rev Rheumatol 2019;15(2):102–12.
[7] Francisco V, Pino J, Gonzalez-Gay MA, Lago F, Karppinen J. Tervonen, O.,et al. A new immunometabolic perspective of intervertebral disc degeneration. Nat Rev Rheumatol 2022;18(1):47–60.
[8] Liu L, He J, Liu C, Yang M, Fu J, Yi. J.,et al. Cartilage intermediate layer protein affects the progression of intervertebral disc degeneration by regulating the extracellular microenvironment (Review). Int J Mol Med 2021; 47: 475-484, 2021.
[9] Vergroesen PP, Kingma I, Emanuel KS, Hoogendoorn RJ, Welting TJ, van Royen B. J.,et al. Mechanics and biology in intervertebral disc degeneration: a vicious circle. Osteoarthritis Cartilage 2015;23(7):1057–70.
[10] Pattappa G, Li Z, Peroglio M, Wismer N, Alini M, Grad S. Diversity of intervertebral disc cells: phenotype and function. J Anat 2012;221(6):480–96.
[11] Zhao Y, Xiang Q, Lin J, Jiang S, Li W. Oxidative stress in intervertebral disc degeneration: new insights from bioinformatic strategies. Oxid Med Cell Longev 2022;2022:2239770.
[12] Feng C., Yang M., Lan M., Liu C., Zhang Y., Huang B.,et al. ROS: crucial intermediators in the pathogenesis of intervertebral disc degeneration. Oxidative medicine and cellular longevity. 2017. p. 1–12. 2017.
[13] Yin H, Wang K, Das A, Li G, Song Y. Luo R.,et al. The REDD1/TXNIP complex accelerates oxidative stress-induced apoptosis of nucleus pulposus cells through the mitochondrial pathway. Oxid Med Cell Longev 2021;2021:7397516.
[14] Xu W, Zhang X, Liu G, Zhu M, Wu Y. Jie Z.,et al. Oxidative stress abrogates the degradation of KMT2D to promote degeneration in nucleus pulposus. Biochim Biophys Acta, Mol Basis Dis 2020;1866(10):165888.
[15] Rajesh D, Dahia CL. Role of sonic hedgehog signaling pathway in intervertebral disc formation and maintenance. Curr Mol Biol Rep 2018;4(4):173–9.
[16] Dahia CL, Mahoney E, Wylie C. Shh signaling from the nucleus pulposus is required for the postnatal growth and differentiation of the mouse intervertebral disc. PLoS One 2012;7(4):e35944.
[17] Sasai N, Toriyama M, Kondo T. Hedgehog signal and genetic disorders. Front Genet 2019;10:1103.
[18] Sigafoos AN, Paradise BD, Fernandez-Zapico ME. Hedgehog/GLI signaling pathway: transduction, regulation, and implications for disease. Cancers 2021;13(14).
[19] Lv T, Shen L, Yang L, Diao W, Yang Z. Zhang Y.,et al. Polydatin ameliorates dextran sulfate sodium-induced colitis by decreasing oxidative stress and apoptosis partially via Sonic hedgehog signaling pathway. Int Immunopharm 2018;64:256–63.
[20] Kaushal JB, Popli P, Sankhwar P, Shukla V, Dwivedi A. Sonic hedgehog protects endometrial hyperplasial cells against oxidative stress via suppressing mitochondrial fission protein dynamin-like GTPase (Drp1). Free Radic Biol Med 2018;129:582–99.
[21] Chen SD, Yang JL, Hwang WC, Yang DI. Emerging roles of sonic hedgehog in adult neurological diseases: neurogenesis and beyond. Int J Mol Sci 2018;19(8).
[22] Avery JT, Zhang R, Boohaker RJ. GLI1: a therapeutic target for cancer. Front Oncol 2021;11:673154.
[23] Yang SH, Hu MH, Wu CC, Chen CW, Sun YH, Yang KC. CD24 expression indicates healthier phenotype and less tendency of cellular senescence in human nucleus pulposus cells. Artif Cells. Nanomed Biotechnol 2019;47(1):3021–8.
[24] Rodrigues-Pinto R, Richardson S, Hoyland J. Identification of novel nucleus pulposus markers: interspecies variations and implications for cell-based therapiesfor intervertebral disc degeneration. Bone & joint research 2013;2(8): 169–78.
[25] Cheng S, Li X, Lin L, Jia Z, Zhao Y. Wang D.,et al. Identification of aberrantly expressed genes during aging in rat nucleus pulposus cells. Stem Cell Int 2019;2019: 2785207.
[26] Moore CB, Guthrie EH, Huang MT, Taxman DJ. Short hairpin RNA (shRNA): design, delivery, and assessment of gene knockdown. Methods Mol Biol 2010;629:141–58.
[27] Che H, Li J, Li Y, Ma C, Liu H. Qin J.,et al. p16 deficiency attenuates intervertebral disc degeneration by adjusting oxidative stress and nucleus pulposus cell cycle. Elife 2020:9.
[28] Schwartzenberg S, Deutsch V, Maysel-Auslender S, Kissil S, Keren G, George J. Circulating apoptotic progenitor cells: a novel biomarker in patients with acute coronary syndromes. Arterioscler Thromb Vasc Biol 2007;27(5):e27–e31.
[29] Pfirrmann C, Metzdorf A, Zanetti M, Hodler J, Boos N. Magnetic resonance classification of lumbar intervertebral disc degeneration. Spine 2001;26(17): 1873–8.
[30] Liebscher T, Haefeli M, Wuertz K, Nerlich AG, Boos N. Age-related variation in cell density of human lumbar intervertebral disc. Spine 2011;36(2):153–9.
[31] Mohanty S, Pinelli R, Pricop P, Albert TJ, Dahia CL. Chondrocyte-like nested cells in the aged intervertebral disc are late-stage nucleus pulposus cells. Aging Cell 2019; 18(5):e13006.
[32] Gao B, Jiang B, Xing W, Xie Z, Luo Z, Zou W. Discovery and application of postnatal nucleus pulposus progenitors essential for intervertebral disc homeostasis and degeneration. Adv Sci 2022;9(13):e2104888.
[33] Xiang Q, Cheng Z, Wang J, Feng X, Hua W. Luo R.,et al. Allicin attenuated advanced oxidation protein product-induced oxidative stress and mitochondrial apoptosis in human nucleus pulposus cells. Oxid Med Cell Longev 2020;2020:6685043.
[34] Balamurugan M, Santharaman P, Madasamy T, Rajesh S, Sethy NK. Bhargava K.,et al. Recent trends in electrochemical biosensors of superoxide dismutases. Biosens Bioelectron 2018;116:89–99.
[35] Park MW, Cha HW, Kim J, Kim JH, Yang H. Yoon S.,et al. NOX4 promotes ferroptosis of astrocytes by oxidative stress-induced lipid peroxidation via the impairment of mitochondrial metabolism in Alzheimer's diseases. Redox Biol 2021; 41:101947.
[36] Zhao C, Wang L, Jiang L, Dai L. The cell biology of intervertebral disc aging and degeneration. Ageing Res Rev 2007;6(3):247–61.
[37] Zhang Y, Yang B, Wang J, Cheng F, Shi K. Ying L.,et al. Cell senescence: a nonnegligible cell state under survival stress in pathology of intervertebral disc degeneration. Oxid Med Cell Longev 2020;2020:9503562.
[38] Buckwalter J. Aging and degeneration of the human intervertebral disc. Spine 1995; 20(11):1307–14.
[39] Dudek M, Yang N, Ruckshanthi JP, Williams J, Borysiewicz E. Wang P.,et al. The intervertebral disc contains intrinsic circadian clocks that are regulated by age and cytokines and linked to degeneration. Ann Rheum Dis 2017;76(3):576–84.
[40] Veras MA, McCann MR, Tenn NA, Seguin CA. Transcriptional profiling of the murine intervertebral disc and age-associated changes in the nucleus pulposus. Connect Tissue Res 2020;61(1):63–81.
[41] Choi KS, Lee C, Harfe BD. Sonic hedgehog in the notochord is sufficient for patterning of the intervertebral discs. Mech Dev 2012;129(9–12):255–62.

[42] Choi K, Harfe B. Hedgehog signaling is required for formation of the notochord sheath and patterning of nuclei pulposi within the intervertebral discs. Proc. Natl. Acad. Sci. U.S.A 2011;108(23):9484–9.
[43] Winkler T, Mahoney EJ, Sinner D, Wylie CC, Dahia CL. Wnt signaling activates Shh signaling in early postnatal intervertebral discs, and re-activates Shh signaling in old discs in the mouse. PLoS One 2014;9(6):e98444.
[44] Bonavita R, Vincent K, Pinelli R, Dahia CL. Formation of the sacrum requires down-regulation of sonic hedgehog signaling in the sacral intervertebral discs. Biol Open 2018;7(7).
[45] Wang J, Ware K, Bedolla A, Allgire E, Turcato FC. Weed M.,et al. Disruption of sonic Hedgehog signaling accelerates age-related neurogenesis decline and abolishes stroke-induced neurogenesis and leads to increased anxiety behavior in stroke mice. Transl Stroke Res 2022 Oct;13(5).
[46] Davalli P., Mitic T., Caporali A., Lauriola A., D'Arca D. ROS, cell senescence, and novel molecular mechanisms in aging and age-related diseases, vol. 2016. Oxid Med Cell Longev; 2016. 3565127.
[47] Zhang X, Huang Z, Xie Z, Chen Y, Zheng Z, Wei X, et al. Homocysteine induces oxidative stress and ferroptosis of nucleus pulposus via enhancing methylation of GPX4. Free radical biology &medicine 2020 Nov 20;160.
[48] Che H, Ma C, Li H, Yu F, Wei Y, Chen H, et al. Rebalance of the polyamine metabolism suppresses oxidative stress and delays senescence in nucleus pulposus cells. Oxid Med Cell Longev 2022;2022:8033353.
[49] Hu S, Zhang C, Qian T, Bai Y, Chen L. Chen J.,et al. Promoting nrf2/sirt3-dependent mitophagy suppresses apoptosis in nucleus pulposus cells and protects against intervertebral disc degeneration. Oxid Med Cell Longev 2021;2021:6694964.
[50] Li Y, Pan D, Wang X, Huo Z, Wu X. Li J.,et al. Silencing ATF3 might delay TBHP-induced intervertebral disc degeneration by repressing NPC ferroptosis, apoptosis, and ECM degradation. Oxid Med Cell Longev 2022;2022:4235126.
[51] Liu Z, Tu K, Wang Y, Yao B, Li Q. Wang L.,et al. Hypoxia accelerates aggressiveness of hepatocellular carcinoma cells involving oxidative stress, epithelial-mesenchymal transition and non-canonical hedgehog signaling. Cell Physiol Biochem : international journal of experimental cellular physiology, biochemistry, and pharmacology 2017;44(5):1856–68.
[52] Dhekne H., Yanatori I., Gomez RC., Tonelli F., Diez F., Schüle B.,et al. A pathway for Parkinson's Disease LRRK2 kinase to block primary cilia and Sonic hedgehog signaling in the brain, vol. 7. eLife; 2018.
[53] He W, Cui L, Zhang C, Zhang X, He J. Xie Y.,et al. Sonic hedgehog promotes neurite outgrowth of cortical neurons under oxidative stress: involving of mitochondria and energy metabolism. Exp Cell Res 2017;350(1):83–90.
[54] Infante P, Alfonsi R, Botta B, Mori M, Di Marcotullio L. Targeting GLI factors to inhibit the Hedgehog pathway. Trends Pharmacol Sci 2015;36(8):547–58.
[55] Meng QH, Liu HB, Wang JB. Polydatin ameliorates renal ischemia/reperfusion injury by decreasing apoptosis and oxidative stress through activating sonic hedgehog signaling pathway. Food Chem Toxicol 2016;96:215–25.
[56] Hess J, Angel P, Schorpp-Kistner M. AP-1 subunits: quarrel and harmony among siblings. J Cell Sci 2004;117(Pt 25):5965–73.
[57] Liu C, Li S, Li Y, Tian J, Sun X. Song T.,et al. Growth hormone ameliorates the age-associated depletion of ovarian reserve and decline of oocyte quality via inhibiting the activation of Fos and Jun signaling. Aging 2021;13(5):6765–81.
[58] Ge R, Wang Z, Zeng Q, Xu X, Olumi AF. F-box protein 10, an NF-kappaB-dependent anti-apoptotic protein, regulates TRAIL-induced apoptosis through modulating c-Fos/c-FLIP pathway. Cell Death Differ 2011;18(7):1184–95.
[59] Zhao Y, Luo A, Li S, Zhang W, Chen H. Li Y.,et al. Inhibitor of differentiation/DNA binding 1 (ID1) inhibits etoposide-induced apoptosis in a c-Jun/c-Fos-dependent manner. J Biol Chem 2016;291(13):6831–42.
[60] Leewananthawet A, Arakawa S, Okano T, Daitoku Kinoshita R, Ashida H. Izumi Y.,et al. Ozone ultrafine bubble water induces the cellular signaling involved in oxidative stress responses in human periodontal ligament fibroblasts. Sci Technol Adv Mater 2019;20(1):589–98.
[61] Ishihara Y, Ito F, Shimamoto N. Increased expression of c-Fos by extracellular signal-regulated kinase activation under sustained oxidative stress elicits BimEL upregulation and hepatocyte apoptosis. FEBS J 2011;278(11):1873–81.
[62] Ali SA, Niu B, Cheah KSE, Alman B. Unique and overlapping GLI1 and GLI2 transcriptional targets in neoplastic chondrocytes. PLoS One 2019;14(1):e0211333.